AN EFFECTIVE THICKNESS TO ESTIMATE STRESSES IN LAMINATED GLASS BEAMS UNDER DYNAMIC LOADINGS

Manuel L. Aenlle[a], F. Pelayo[a*] and G. Ismael[a]

[a]Department of Construction and Manufacturing Engineering, University of Oviedo, Campus de Gijón, Zona Oeste, Edificio 7, 33203, Gijón, Spain.

[*]corresponding author; E-mail: fernandezpelayo@uniovi.es
Phone: +34985181932

ABSTRACT

Finite element models for estimating stresses and displacements in laminated glass elements under dynamic loadings are very time-consuming because (1) many small 3D elements are needed to model accurately all the layers of the sandwich element and (2) the core usually shows a time and temperature dependent behaviour. In the last years, the concept of effective thickness using a quasi-elastic solution has got the attention of the research community because of its simplicity and reasonable level of accuracy achieved in the calculation of laminated glass elements under static loadings. In this paper, a dynamic effective thickness to estimate stresses in laminated glass beams under dynamic loadings in the frequency domain is derived using the correspondence principle. The analytical equations are validated by experimental tests carried out on simply supported and free-free laminated glass beams at different temperatures in the range 20-40ºC.

KEYWORDS: A. Layered Structures ; B. Vibration ; C. Analytical modelling ; D. Thermal analysis.

NOMENCLATURE

E	Young modulus
E_{eff}	Effective Young modulus
E_1	Young's modulus of glass layer 1
E_3	Young's modulus of glass layer 3
$E_2^*(\omega)$	Complex tensile modulus for the polymeric interlayer
$E_2'(\omega)$	Real component of the tensile complex modulus (storage)
$E_2''(\omega)$	Imaginary component of the tensile complex modulus (loss)
$E_2(t)$	Viscoelastic relaxation tensile modulus for polymeric interlayer
$G_2(t)$	Viscoelastic relaxation shear modulus for the polymeric interlayer
$G_2^*(\omega)$	Complex shear modulus for the polymeric interlayer
$G_2'(\omega)$	Real component of the shear complex modulus (storage)
$G_2''(\omega)$	Imaginary component of the shear complex modulus (loss)
H_1	Thickness of glass layer 1 in laminated glass
H_2	Thickness of polymeric layer in laminated glass
H_3	Thickness of glass layer 3 in laminated glass
$H_0 = H_2 + \left(\frac{H_1 + H_3}{2}\right)$	
I	Second moment of area
$I_1 = \frac{H_1^3}{12}$	

$I_3 = \frac{H_3^3}{12}$

$I_T = I_1 + I_3 = \frac{H_1^3 + H_3^3}{12}$

$K_2(t)$ Viscoelastic bulk modulus

$K_2^*(\omega)$

L Length of a glass beam

T Temperature

T_0 Reference temperature

$Y = \frac{H_0^2 E_1 H_1 E_3 H_3}{EI_T(E_1 H_1 + E_3 H_3)}$

LOWERCASE LETTERS

a_T Shift factor

b Width of a glass beam

$g(x)$ Shape function (Galuppi and Royer Carfagni model)

i Imaginary unit

k_I Wavenumber

$\overline{m}$ Mass per unit area

t Time

w Deflection

GREEK LETTERS

Ω^*	Non-dimensional complex frequency
ζ	Modal damping ratio
η	Loss factor
η_2	Loss factor of the polymeric interlayer of laminated glass
ρ_i	Mass density of laminated glass layers
ω	Frequency

1 INTRODUCTION

Laminated glass is a sandwich or layered material which consists of two or more plies of monolithic glass with one or more interlayers of a polymeric material. All polymeric interlayers present a viscoelastic behaviour, i.e. their mechanical properties are frequency (or time) and temperature dependent [1, 2]. Polyvinyl butyral (PVB) is the most used interlayer material.

In analytical and numerical models, glass mechanical behaviour is usually modelled as linear-elastic in the pre glass-breakage, whereas the polymeric interlayer is characterized as linear-viscoelastic [1]. Laminated glass is easy to assemble in a finite element models but a lot of small 3D elements are needed to mesh accurately because the thickness of the viscoelastic interlayer is usually very small compared with the dimension of the laminated glass element. Consequently, the 3D models are highly time-consuming.

In the last years several analytical models have been proposed for determining the static deflections and stresses of laminated glass beams [2, 3, 4, 5, 6, 7, 8]. In order to simplify the calculation of deflections and stresses in laminated glass beams, the concept of effective thickness have been proposed in the literature [7, 8]. The method consists of calculating the thickness (time and temperature dependent) of a monolithic element with bending properties equivalent to those of the laminated one, that is to say, the deflections and stresses provided by the equivalent monolithic beam are equal to those of the layered model with viscoelastic core.

With respect to the dynamic behaviour, several models were proposed in the 60's and 70's about the dynamic flexural vibration of sandwich beams with viscoelastic core [9, 10, 11, 12, 13, 14]. Aenlle and Pelayo [15] demonstrated that the model of Ross, Kerwin and Ungar (RKU) [9] can be considered as a particular case of the Mead and Markus model [12] when the exponential decay rate per unit length along the beam is neglected. The authors derived an effective stiffness for the dynamic behavior of laminated glass beams from the RKU model [9], which can be used to calculate modal parameters and dynamic deflections in laminated glass beams. With this technique, monolithic numerical models with an effective stiffness [17, 18] can be used advantageously in place of layered models.

A dynamic effective thickness for laminated glass plates was proposed by Aenlle and Pelayo [16]. Furthermore, the authors proposed the effective Young modulus concept for beams and plates which is more attractive for using in numerical models. The effect of temperature in the dynamic behaviour of laminated glass elements was studied in [15, 16, 19].

The aim of this paper is to propose a simplified method to estimate stresses in the frequency domain in laminated glass beams subject to dynamic loadings using an equivalent monolithic model, avoiding the use of layered finite element models or complicated analytical models. A dynamic stress effective thickness for laminated glass beams in the frequency domain is derived by applying the correspondence principle [20, 21, 22, 23] to the stress effective thickness for static loadings proposed by Galuppi and Royer Carfagni [8]. The dynamic stress effective thickness is dependent on the dynamic effective stiffness proposed by Aenlle and Pelayo [15, 16] to estimate modal parameters and dynamic deflections. Equations for the stress effective Young Modulus and the stress effective distance to the neutral axis are also formulated which can be used in place of the effective thickness with the same accuracy. This technique can be applied to three layered laminated glass beams with glass showing a linear elastic behaviour and the polymeric core showing viscoelastic behaviour [1, 20, 21, 22, 23]. In order to validate the model, the stresses in a laminated glass beam made of annealed glass plies and PVB core were estimated using the stress effective thickness concept. The analytical predictions were validated with experimental tests comparing the predicted stresses with those measured with strain gages.

2.1 VISCOELASTIC BEHAVIOUR

The mechanical properties of a linear-viscoelastic material are frequency (or time) and temperature dependent [1, 22]. In the frequency domain, the complex tensile modulus, $E_2^*(\omega)$, at temperature T is given by:

$$E_2^*(\omega,T) = E_2'(\omega,T) + i \cdot E_2''(\omega,T) = E_2'(\omega,T)(1 + i \cdot \eta_2(\omega,T)) \quad (1)$$

where superscript '*' indicates complex, ω represents the frequency, i is the imaginary unit, $E_2'(\omega,T)$ and $E_2''(\omega,T)$ are the storage and the loss tensile moduli, respectively, and

$$\eta_2(\omega) = \frac{E_2''(\omega,T)}{E_2'(\omega,T)} \tag{2}$$

is the loss factor that relates both moduli. The subscript '2' is used hereafter to reference the viscoelastic interlayer (Figure 1).

As regards the shear behavior, the complex shear modulus, $G_2^*(\omega,T)$, is given by:

$$G_2^*(\omega,T) = G_2'(\omega,T) + i \cdot G_2''(\omega,T) = G_2'(\omega,T)(1 + i \cdot \eta_2(\omega,T)) \tag{3}$$

where $G'(\omega,T)$ and $G''(\omega,T)$ are the storage and the loss shear moduli, respectively.

Both the shear and tensile moduli can be related by means of the correspondence principle [20, 21, 22, 23] introducing the corresponding complex viscoelastic properties, i.e.:

$$G_2^*(\omega,T) = \frac{3E_2^*(\omega,T)\,K_2^*(\omega,T)}{9K_2^*(\omega,T) - E_2^*(\omega,T)} \tag{4}$$

where $K_2^*(\omega,T)$ is the complex bulk modulus.

In order to take into account the temperature dependence of the viscoelastic interlayer properties, it is commonly assumed a simply thermo-rheological behaviour in the material [22]. This fact allows determining a relation between time and temperature in linear viscoelastic materials using a Time-Temperature-Superposition (TTS) model such as the William-Landel-Ferry or Arrhenius equations [1, 24]. Once the TTS model is fitted for a reference temperature, T_0, i.e. the temperature used in the experimental tests, the moduli for the material to a different temperature, T_1, can be estimated by

shifting in time the moduli at temperature T_0 using a shift factor, $a_T(T_0, T_1)$, obtained from the material TTS model. A similar process can be followed in the frequency domain [23, 24].

2.2 GALUPPI AND ROYER-CARFAGNI MODEL

Galuppi and Royer-Carfagni [8, 25, 26] derived a model for calculating the deflection of laminated glass beams under static loading that can be applied to a very wide range of boundary and loading conditions. The deflection of the beam is given by:

$$w(x,t,T) = -\frac{g(x)}{EI(t,T)_S} \tag{5}$$

where g(x) is a shape function that takes the form of the elastic deflection of a monolithic beam with constant cross section under the same loading and boundary conditions as the laminated glass beam and $EI(t)_S$ is the effective bending stiffness of the laminated glass beam given by:

$$\mathrm{EI(t,T)_S} = \frac{1}{\frac{\eta_S(\mathrm{t,T})}{\mathrm{EI_T}(1+\mathrm{Y})} + \frac{1-\eta_S(\mathrm{t,T})}{\mathrm{EI_T}}} \tag{6}$$

Where:

$$\eta_S(t,T) = \frac{1}{1 + \frac{E_1 H_1 H_2 E_3 H_3 \psi_B}{(1+\mathrm{Y})\mathrm{G}_2(t,T)(E_1 H_1 + E_3 H_3)}} \tag{7}$$

In [16] it was demonstrated that that the parameter ψ_B is related to the wavelength of the first buckling mode shape, λ_{1bck} , by means of:

$$\psi_B = \frac{4\pi^2}{\lambda_{1bck}^2} \tag{8}$$

The parameter $\eta_S(t)$ takes values in the range $0 \leq \eta_S(t) \leq 1$ corresponding $\eta_S = 0$ to the case of a layered beam and $\eta_S = 1$ to a monolithic beam.

The stresses in each glass ply are given as the summation of the contribution of axial forces and bending moments. The stresses at the top and the bottom of layer 1 are given by [8]:

$$\sigma_1(x,t,T) = \left(\underbrace{E_1 \eta_s(t,T) \cdot \frac{EI(t,T)_s}{EI_{TOT}} \frac{H_3 H_0}{H_1 + H_3}}_{axial} \pm \underbrace{\frac{E_1 H_1}{2}}_{bending} \right) w''(x,t,T) \tag{9}$$

whereas for layer 3 are given by:

$$\sigma_3(x,t,T) = \left(\underbrace{-E_3 \eta_s(t,T) \cdot \frac{EI(t,T)_s}{EI_{TOT}} \frac{H_0 H_1}{H_1 + H_3}}_{axial} \pm \underbrace{\frac{E_3 H_3}{2}}_{bending} \right) w''(x,t,T) \tag{10}$$

Where superscript $''$ indicates second derivative of the deflection shape with respect to x.

2.3 STATIC EFFECTIVE THICKNESS

The static deflection-effective thickness is defined as the thickness of a monolithic glass with the same width and length, which gives the same displacement as does the laminated-glass beam under the same loading [7, 8, 25]. As the behaviour of the laminated glass elements are time and temperature dependent, an effective thickness has to be determined for each time and temperature. The deflection effective thickness for laminated glass beams can be determined identifying the stiffness of a monolithic beam with Young modulus E_i and thickness H_{ieff} with the stiffness given by Eq. (6), i.e.:

$$\frac{E_i H_{ieff}^3(t,T)}{12} = \mathrm{EI(t,T)_S} \tag{11}$$

where the subindex "$_{\mathrm{eff}}$" indicates effective. From Eq. (11) it is derived that:

$$H_{1eff}(\mathrm{t},\mathrm{T}) = \sqrt[3]{\frac{12EI_T(1+Y)}{E_1\left(1+Y(1-\eta_S(t))\right)}} \tag{12}$$

and

$$H_{3eff}(\mathrm{t},\mathrm{T}) = \sqrt[3]{\frac{12EI_T(1+Y)}{E_3\left(1+Y(1-\eta_S(t))\right)}} \tag{13}$$

An effective Young modulus E_{eff} can easily be derived from:

$$\frac{E_{eff}(t)H^3}{12} = \mathrm{EI(t)_S} \tag{14}$$

which results in:

$$E_{eff}(\mathrm{t},\mathrm{T}) = \frac{12EI_T(1+Y))}{H^3\left(1+Y(1-\eta_S(t))\right)} \tag{15}$$

where

$$H = H_1 + H_2 + H_3 \tag{16}$$

With respect to the stresses, the stress-effective thickness of a laminated-glass beam ply is defined as the thickness of a monolithic glass beam that, under the same boundary and load conditions of the problem at hand, presents the same maximum stress [7, 8].

The stress-effective thickness for layer 1, $\mathrm{H_{1\sigma eff}}$, is obtained equating Eq. (9) with the equation:

$$\sigma_1(x,t,T) = \frac{EI(t,T)_s}{\frac{H_{1\sigma eff}^2}{6}} w''(x,t,T) \tag{17}$$

Which results in:

$$H_{1\sigma eff}(t,T) = \sqrt{\frac{1}{\frac{E_1\eta_s(t,T)H_3H_0}{6EI_{TOT}(H_1+H_3)} + \frac{H_1}{H_{1eff}^3(t,T)}}} \tag{18}$$

The same procedure is followed to derive the stress-effective thickness for layer 3, $H_{3\sigma eff}$, which is expressed as:

$$H_{3\sigma eff}(t,T) = \sqrt{\frac{1}{\frac{E_3\eta_s(t,T)H_1H_0}{6EI_{TOT}(H_1+H_3)} + \frac{H_3}{H_{3eff}^3(t,T)}}} \tag{19}$$

2.4 DYNAMIC EFFECTIVE STIFFNESS

Ross, Kerwin, and Ungar [9, 27] developed a model for the flexural vibrations of sandwich elements considering the beam simply supported and assuming a flexural deformation spatially sinusoidal in shape, which is formulated as:

$$EI^*(\omega,T)\, w(x,t,T)^{IV} + \bar{m}\, \ddot{w}(x,t,T) = 0 \tag{20}$$

Where $\bar{m}$ is the mass per unit length and $EI^*(\omega,T)$ is an effective complex flexural stiffness given by:

$$EI^*(\omega,t) = \frac{1}{\frac{\eta_d(\omega,T)}{EI_T(1+Y)} + \frac{1-\eta_d(\omega,T)}{EI_T}} \tag{21}$$

where

$$\eta_d(\omega,T)=\frac{1}{1+\frac{E_1\,H_1\,H_2E_3\,H_3\;\;k_I^2(\omega,T)}{G_2^*\,(\omega,T)(E_1H_1+E_3H_3)(1+Y)}} \tag{22}$$

And $k_I(\omega,T)$ is the wavenumber, which is related with the wavelength $\lambda(\omega,T)$ by means of:

$$k_I(\omega,T)=\frac{2\pi}{\lambda(\omega,T)} \tag{23}$$

The complex natural frequencies are estimated with the expression:

$$\omega^2(1+i\cdot\eta)=k_I^4(\omega,T)\frac{EI^*(\omega,T)}{\overline{m}} \tag{24}$$

The dynamic effective thickness and the dynamic effective Young modulus are derived using the same methodology as that used in statics and they are expressed as [15, 16]:

$$H_{1eff}(\omega,T)=\sqrt[3]{\frac{12EI_T(1+Y)}{E_1\left(1+Y\left(1-\eta_d(\omega,T)\right)\right)}} \tag{25}$$

$$H_{3eff}(\omega,T)=\sqrt[3]{\frac{12EI_T(1+Y)}{E_3\left(1+Y\left(1-\eta_d(\omega,T)\right)\right)}} \tag{26}$$

$$E_{eff}(\omega,T)=\frac{12EI_T(1+Y))}{H^3\left(1+Y\left(1-\eta_d(\omega,T)\right)\right)} \tag{27}$$

3 DYNAMIC EFFECTIVE THICKNESS FOR STRESSES

The correspondence principle [20, 21, 22, 23] states that if a solution to a linear elasticity problem is known, the solution to the corresponding problem for a linearly viscoelastic material can be obtained by replacing each quantity which can depend on frequency by its Fourier Transform.

The dynamic stiffness in the frequency domain given by Eq. (21) can be derived from the static stiffness (Eq. (6)) by means of the Correspondence Principle [20, 21, 22, 23]. The same can be said for the dynamic effective thickness (Eqs. 25 and 26), which can be derived from Eqs. (12) and (13), and the effective Young modulus (Eq. 27) which can be obtained from Eq. (15).

With respect to parameter $\eta_d(\omega, T)$, it can also be derived from $\eta_s(t, T)$ with the correspondence principle but with the special feature that the wavelength of the first buckling mode shape, λ_{1bck}, must be replaced with the wavelength of the vibration mode shape $\lambda(\omega, T)$.

We are going to apply hereafter the correspondence principle to derive equations for estimating stresses in the frequency domain, as well as equations for the dynamic stress effective thickness, the dynamic stress effective distance to neutral axis, and the dynamic stress Young modulus.

Equations for estimating stresses in the frequency domain can be derived from equations (9) and (10) applying the correspondence principle. The stresses at the top and bottom of layer 1 are given by:

$$\sigma_1(x,\omega,T) = E_1 \left[\underbrace{\eta_d(\omega,T) \cdot \frac{EI^*(\omega,T)}{EI_{TOT}} \frac{H_3}{H_1+H_3} \cdot H_0}_{axial} \pm \underbrace{\frac{H_1}{2}}_{bending} \right] \cdot w''(x,\omega,T) \qquad (28)$$

And for layer 3 by:

$$\sigma_3(x,\omega,T) = -E_3 \left[\underbrace{\eta_d(\omega,T) \cdot \frac{EI^*(\omega,T)}{EI_{TOT}} \frac{H_1}{H_1+H_3} \cdot H_0}_{axial} \pm \underbrace{\frac{H_3}{2}}_{bending} \right] \cdot w''(x,\omega,T) \qquad (29)$$

The dynamic effective stiffness $EI^*(\omega,T)$ given by Eq. (21) was derived by Aenlle and Pelayo [15, 16] from the Mead and Markus model [12].

If we take into account that:

$$\eta_d(\omega,T)\cdot\frac{EI^*(\omega,T)}{EI_{TOT}}=\frac{1}{Y}\left(\frac{EI^*(\omega,T)}{EI_T}-1\right) \tag{30}$$

Eqs. (28) and (29) are simplified to:

$$\sigma_1(x,\omega,T)=E_1\left[\underbrace{\frac{1}{Y}\left(\frac{EI^*(\omega,T)}{EI_T}-1\right)\frac{H_3}{H_1+H_3}\cdot H_0}_{axial}\pm\underbrace{\frac{H_1}{2}}_{bending}\right]\cdot w''(x,\omega,T) \tag{31}$$

And:

$$\sigma_3(x,\omega,T)=-E_3\left[\underbrace{\frac{1}{Y}\left(\frac{EI^*(\omega,T)}{EI_T}-1\right)\frac{H_1}{H_1+H_3}\cdot H_0}_{axial}\pm\underbrace{\frac{H_3}{2}}_{bending}\right]\cdot w''(x,\omega,T) \tag{32}$$

As regarding the dynamic stress effective thicknesses, they are obtained applying the correspondence principle to Eqs. (18) and (19) and they are expressed as:

$$H_{1\sigma eff}(\omega,T)=\sqrt{\frac{1}{\frac{E_1\eta_d(\omega,T)H_3H_0}{6EI_{TOT}(H_1+H_3)}+\frac{H_1}{H_{1eff}^3(\omega,T)}}} \tag{33}$$

for layer 1 and

$$H_{3\sigma eff}(\omega,T)=\sqrt{\frac{1}{\frac{E_3\eta_d(\omega,T)H_1H_0}{6EI_{TOT}(H_1+H_3)}+\frac{H_3}{H_{3eff}^3(\omega,T)}}} \tag{34}$$

for layer 3.

Assuming constant Young modulus E_1 for layer 1 and E_3 for layer 3, expressions for the dynamic stress effective distances to neutral axis $\mathrm{h}_{1\sigma\mathrm{eff}}(\omega,\mathrm{T})$ and $\mathrm{h}_{3\sigma\mathrm{eff}}(\omega,\mathrm{T})$ can be easily formulated from Eqs. (28) and (29), which results in:

$$h_{1\sigma eff}(\omega,T)=\eta_d(\omega,T)\cdot\frac{EI^*(\omega,T)}{EI_{TOT}}\,\frac{H_3}{H_1+H_3}\cdot H_0+\frac{H_1}{2} \tag{35}$$

for layer 1,and in:

$$h_{1\sigma eff}(\omega,T)=\eta_d(\omega,T)\cdot\frac{EI^*(\omega,T)}{EI_{TOT}}\,\frac{H_3}{H_1+H_3}\cdot H_0+\frac{H_3}{2} \tag{36}$$

for layer 3.

The same expressions given by Eqs. (35) and (36) can also be obtained from:

$$\mathrm{h}_{1\sigma\mathrm{eff}}(\omega,\mathrm{T})=\frac{H_{1eff}^3}{2H_{1\sigma eff}^2} \tag{37}$$

and

$$\mathrm{h}_{3\sigma\mathrm{eff}}(\omega,\mathrm{T})=\frac{H_{3eff}^3}{2H_{3\sigma eff}^2} \tag{38}$$

, respectively. Dynamic stress effective Young modulus can also be derived from Eqs. (28) and (29). The stress effective Young modulus for layer 1 with thickness H_1, is expressed as:

$$E_{1\sigma eff}(\omega,T)=E_1\left[\eta_d(\omega,T)\cdot\frac{EI^*(\omega,T)}{EI_{TOT}}\frac{H_3H_0}{H_1+H_3}\cdot\frac{2}{H_1}+1\right] \tag{39}$$

And for layer 3 with thickness H_3 as:

$$E_{3\sigma eff}(\omega,T)=E_3\left[\eta_d(\omega,T)\cdot\frac{EI^*(\omega,T)}{EI_{TOT}}\frac{H_1H_0}{H_1+H_3}\cdot\frac{2}{H_1}+1\right] \tag{40}$$

3.1 PRACTICAL APPLICATION

The three concepts described in the previous section for estimating dynamic stresses in laminated glass beams (effective thickness, effective distance to neutral axis and effective Young modulus) can be used interchangeable without losing of accuracy.

If the bending moment distribution $M(x)$ is known, the stresses can be estimated using the effective thickness concept with the equations:

$$\sigma_1(x,\omega,T) = \frac{M(x)}{\frac{H_{1\sigma eff}(\omega,T)}{6}} \tag{41}$$

and

$$\sigma_3(x,\omega,T) = \frac{M(x)}{\frac{H_{3\sigma eff}(\omega,T)}{6}} \tag{42}$$

respectively.

However, if the curvature $w''(x,\omega,T)$ of the beam is known (from experimental measurements, from analytical calculations, numerical models, etc.) the dynamic effective distance to the neutral axis $h_{i\sigma eff}$ can be used with the equations:

$$\sigma_1(x,\omega,T) = E_1\, h_{1\sigma eff}(\omega,T) \cdot w''(x,\omega,T) \tag{43}$$

and

$$\sigma_3(x,\omega,T) = E_3\, h_{3\sigma eff}(\omega,T) \cdot w''(x,\omega,T) \tag{44}$$

With respect to the dynamic effective Young modulus $E_{i\sigma eff}$, it can be used with the equations:

$$\sigma_1(x,\omega,T) = E_{1eff}(\omega,T)\, H_1 \cdot w''(x,\omega,T) \tag{45}$$

and

$$\sigma_3(x,\omega,T) = E_{3eff}(\omega,T)\, H_3 \cdot w''(x,\omega,T) \tag{46}$$

3.2 MONOLITHIC FE MODELS

The concept of effective thickness is based on using a monolithic model with constant Young modulus and a frequency and temperature dependent thickness. However, if we intend to assemble a monolithic FEM for calculating stresses in laminated glass beams, it is more appealing to use a beam with constant thickness and a frequency and temperature dependent Young modulus. Thus, the monolithic model must be defined with:

- Constant thickness $H = H_1 + H_2 + H_3$
- Constant density $\rho_{eq} = \frac{\rho_1 H_1 + \rho_2 H_2 + \rho_3 H_3}{H_1 + H_2 + H_3}$
- Dynamic effective Young modulus $E_{eff}(\omega, T)$ given by Eq. (27)

This equivalent monolithic model provides the same modal parameters as the laminated glasss beam and, consequentely, the same curvatures, i.e.:

$$w''_{LAM}(x, \omega, T) = w''_{MON}(x, \omega, T) \tag{47}$$

Where sub-indexes "LAM" and "MON" indicates laminated and monolithic, respectively.

Thus, using the curvatures obtained with the equivalent monolithic model, the stresses in a laminated glass beam can be estimated with:

$$\sigma_{1LAM}(x, \omega, T) = E_1 \left[\underbrace{\eta_d(\omega, T) \cdot \frac{EI^*(\omega, T)}{EI_{TOT}} \frac{H_3}{H_1 + H_3} \cdot H_0}_{axial} \pm \underbrace{\frac{H_1}{2}}_{bending} \right] \cdot w''_{MON}(x, \omega, T) \tag{48}$$

For layer 1 and with:

$$\sigma_{3LAM}(x, \omega, T) = -E_3 \left[\underbrace{\eta_d(\omega, T) \cdot \frac{EI^*(\omega, T)}{EI_{TOT}} \frac{H_1}{H_1 + H_3} \cdot H_0}_{axial} \pm \underbrace{\frac{H_3}{2}}_{bending} \right] \cdot w''_{MON}(x, \omega, T) \tag{49}$$

for layer 3.

An alternative consists of considering the stresses $\sigma_{MON}(x, \omega, T)$ calculated with the equivalent monolithic FE model, which are related to the curvature by:

$$\sigma_{MON}(x, \omega, T) = E_{eff}(\omega, T) \cdot \frac{H}{2} \cdot w''_{MON}(x, \omega, T) \tag{50}$$

and then to estimate the stresses in the laminated glass beam by means of:

$$\sigma_{1LAM}(x,\omega,T) = \sigma_{MON}(x,\omega,T) \cdot \frac{E_1\left[\eta_d(\omega,T) \cdot \frac{EI^*(\omega,T)}{EI_{TOT}} \frac{H_3}{H_1+H_3} \cdot H_0 \pm \frac{H_1}{2}\right]}{E_{eff}(\omega,T) \cdot \frac{H}{2}} \quad (51)$$

which is obtained identifying Eqs. (28) and (47). Eq. (51) can also be expressed as:

$$\sigma_{1LAM}(x,\omega,T) = \sigma_{MON}(x,\omega,T) \cdot \frac{E_1 \mathrm{h}_{1\sigma\mathrm{eff}}(\omega,\mathrm{T})}{E_{eff}(\omega,T) \cdot \frac{H}{2}} = \sigma_{MON}(x,\omega,T) \cdot \frac{E_{1\sigma eff}(\omega,\mathrm{T}) \cdot H_1}{E_{eff}(\omega,T) \cdot H} \quad (52)$$

With respect to layer 3, the stresses are estimated with:

$$\sigma_{3LAM}(x,\omega,T) = \sigma_{MON}(x,\omega,T) \cdot \frac{E_3\left[\eta_d(\omega,T) \cdot \frac{EI^*(\omega,T)}{EI_{TOT}} \frac{H_1}{H_1+H_3} \cdot H_0 \pm \frac{H_3}{2}\right]}{E_{eff}(\omega,T) \cdot \frac{H}{2}} \quad (53)$$

or:

$$\sigma_{3LAM}(x,\omega,T) = \sigma_{MON}(x,\omega,T) \cdot \frac{E_3 \mathrm{h}_{3\sigma\mathrm{eff}}(\omega,\mathrm{T})}{E_{eff}(\omega,T) \cdot \frac{H}{2}} = \sigma_{MON}(x,\omega,T) \frac{E_{3\sigma eff}(\omega,\mathrm{T}) \cdot H_3}{E_{eff}(\omega,T) \cdot H} \quad (54)$$

3.3 USING EXPERIMENTAL DATA

If modal analysis is applied to the laminated glass beam in order to estimate the modal parameters (natural frequencies, mode shapes and damping ratios), and the experimental response time histories $\mathrm{w_{ex}(t,T)}$are measured at several points of the structure, the experimental modal coordinates $\mathrm{q_{ex}}(\omega,\mathrm{T})$ can be estimated by:

$$q_{ex}(\omega,T) = \phi_{ex}^{-1}(x) w_{ex}(x,\omega,T) \quad (55)$$

Where subscript "ex" indicates experimental data and ϕ_{ex}^{-1} represents the inverse matrix of the experimental mode shapes. The pseudoinverse must be used if the matrix ϕ_{ex} is not square [28, 29].

On the other hand, the experimental mode shapes can be expanded using one of the techniques proposed in the literature [29, 30], from which the curvatures at any point of the structure are estimated by:

$$w''(x,\omega,T) = \phi''_{xp}(x) \cdot q_{ex}(\omega,T) \tag{56}$$

where the subindex 'xp' indicates expanded. If Eq. (56) is substituted in Eq. (28), the stresses at any point of the layer 1 can be obtained with the expression:

$$\sigma_1(x,\omega,T) = E_1 \left[\eta_d(\omega,T) \cdot \frac{EI^*(\omega,T)}{EI_{TOT}} \frac{H_3}{H_1+H_3} \cdot H_0 \pm \frac{H_1}{2} \right] \cdot \sum_{i=1}^{Nmodes} \phi''_{ixp}(x) \cdot q_{iex}(\omega,T) \tag{57}$$

whereas the expression for estimating stresses in layer 3 is given by:

$$\sigma_3(x,\omega,T) = -E_3 \left[\eta_d(\omega,T) \cdot \frac{EI^*(\omega,T)}{EI_{TOT}} \frac{H_1}{H_1+H_3} \cdot H_0 \pm \frac{H_3}{2} \right] \cdot \sum_{i=1}^{Nmodes} \phi''_{ixp}(x) \cdot q_{iex}(\omega,T) \tag{58}$$

which is obtained substituting Eq. (56) in Eq. (29).

Moreover, we can also take advantage of the experimental modal parameters to improve the accuracy of the technique, replacing the stiffness $EI^*(\omega, T)$ in Eqs. (57) and (58) by its equivalent experimental modal equation, i.e.:

$$EI^*(\omega_{ex},T) = \frac{\omega(T)^2_{ex}(1 + i \cdot \eta(T)_{ex}) \cdot (\rho_1 H_1 + \rho_2 H_2 + \rho_3 H_3)}{k_I^4(\omega_{ex},T)} \tag{59}$$

Where $\omega(T)_{ex}$ and $\eta(T)_{ex}$ are the experimental natural frequencies and loss factors at temperature T, respectively.

4. VALIDATION OF THE METHODOLOGY

In order to validate the technique proposed in this paper, the stresses of a laminated glass beam with annealed glass layers, PVB core and with the following geometrical data: $L = 1$ m, $H_1 = 3.75$ mm, $H_2 = 0.38$ mm, $H_3 = 7.90$ mm, $b = 0.1$ m, were predicted using the Eqs. (57) and (58) and validated with experimental tests. The beam was tested in simply supported and in free-free boundary conditions at temperatures in the range $20 - 40\ ^oC$. For temperatures below $20\ ^oC$ the mechanical behaviour of the laminated glass beam is similar to a monolithic glass beam [15, 16, 19] and the technique is equal to or more accurate than the corresponding one at $20\ ^oC$.

4.1. OPERATIONAL MODAL ANALYSIS

The experimental modal parameters at different temperatures were identified with operational modal analysis OMA, which is a technique that allows us to estimate the model parameters (natural frequencies, mode shapes and damping ratios) without knowing and/or controlling the input excitation [31]. The experimental tests were carried out at different temperatures in a climate chamber. The beam was excited applying many small hits along the beam with an impact hammer, random in time and space [31]. The responses were measured using seven uniformly distributed accelerometers with a sensitivity of 100 mV/g, during a period of approximately 4 minutes. The test setup is shown in Figure 2 where the arrows indicate the measured directions. The responses were recorded with a sampling frequency of 2132 Hz using a National Instruments Compact DAQ acquisition system equipped with NI9234 acceleration modules.

The modal parameters were estimated with the frequency-domain decomposition (EFDD) [32] and the stochastic subspace iteration (SSI) [33] methods. The two techniques provide similar results and, therefore, only the modal parameters estimated with the EFDD technique are presented. The identified natural frequencies and loss factors corresponding to the first 3 modes are presented in Tables 1 and 2 for simply supported and free-free boundary conditions, respectively. For the loss factor, η, it has been assumed that $\eta = 2\,\zeta$ [34].

4.2 STRESS MEASUREMENTS

Two strain gages HBM LY11-350 were attached at points 1 and 2 (see Figure 2). In order to excite the structure, several hits were applied to the beam in random positions using an impact hammer and the acceleration responses were recorded using the same test setup as that used for OMA. Both accelerations and strains were acquired using the National Instruments Compact DAQ acquisition system.

4.3 STRESS ESTIMATION

The stresses at the points where the strain gages were attached (see Figure 2) were estimated using the methodology described in the previous section (Eqs. (57) and (58)).

A Young modulus of 72 GPa and a Poisson ratio $\nu = 0.22$, respectively, were considered for the glass layers whereas the mechanical properties obtained with a DTMA in a previous work [35] were considered for the PVB.

A monolithic finite element model was also assembled in ABAQUS and the beam was discretized using 8 Euler-Bernoulli beam elements. The experimental mode shapes were expanded to the un-measured DOF's using the numerical mode shapes extracted from the FEM using the Local Correspondence Principle [29]. The number of numerical modes considered in the expansion of the experimental mode shapes, as well as the contribution of each mode, are presented in Table 3.

The experimental modal coordinates were obtained using Eq. (55) considering the experimental mode shapes at $T = 20\,^{o}C$. This assumption is reasonable because not significant changes in mode shapes with temperature have been observed in previous works [15, 16, 19]. The experimental modal coordinates were filtered using a high pass filter and the integration was carried using a rectangular window with a 50% of overlap [28].

5 DISCUSSION OF THE RESULTS

5.1 SIMPLY SUPPORTED BEAM

The time histories and the power spectral densities (PSD) of the experimental stresses measured with a strain gage located at the midpoint of the beam (point 1 in Figure 2) in the simply supported configuration, and those predicted with Eqs. (57) and (58) at temperatures of 20 ^{o}C, 30 ^{o}C and 40 ^{o}C, are presented in Figure 3. The stresses in time domain were computed by inverse Fourier Transform [36]. It can be observed that the noise floor of the experimental strain gage is approximately 60 dB at all the tested temperatures.

Due to the fact that the strain gage is located in the mid-point of the beam only the peaks corresponding to symmetric modes appear in the spectral densities, i.e., only the modes 1 and 3 contribute to the overall stress at this point in this frequency range. This fact is in agreement with the stresses recorded with the strain gage where the main contributions also correspond to modes 1 and 3 (see Figure 3). With respect to the influence of the temperature, the contribution of the 3rd mode decreases with temperature.

From Figure 3 it is inferred that the stresses are predicted with a good accuracy at 20 ºC and 30 ºC, the error being less than 9% for the first natural frequency. At 40 ºC the stresses at the first mode are predicted with an error of 19%. The errors between the estimated and the experimental power spectral density of the stresses at the first natural frequency (area under the power spectral density at the first natural frequency) are presented in Table 4. As it is demonstrated with the free-free tests, this lack of accuracy is not a problem of the technique but due to the fact that the mechanical properties of the PVB have not been estimated with the required accuracy.

The experimental and the predicted power spectral densities of the stresses at point 2 are presented in figure 4 together with the corresponding time histories. It can be observed that the first three modes contribute to the overall stress in the frequency range 0-500 Hz. The errors between the estimated and the experimental power spectral density of the stresses at the first natural frequency are less than 9% and they are presented in Table 4.

5.2 FREE-FREE BEAM

With respect to the free-free beam tests, the time histories and the spectral densities of the experimental and the estimated stresses at the mid-point of the beam for temperatures $T = 20\,^{o}\mathrm{C}$, $30\,^{o}\mathrm{C}$ and $40\,^{o}\mathrm{C}$ are presented in Figure 5. Beside the peaks corresponding to modes 1 and 3, some peaks at 50 Hz and its harmonics (100 Hz, 150 Hz, 200 Hz and so on) corresponding to electrical noise are also present in the spectral densities, which could not be removed during the tests.

As in the simply-supported conditions, only the first and the third mode contribute to the overall stress at this point. Again the error between the experimental and the predicted power spectral densities of the stresses at the first natural frequency increases with temperature. The errors at the first natural frequency are presented in Table 4 and they are of the same order as those obtained for the simply supported beam.

As it was shown in Section 3.3, the accuracy of the technique can be improved replacing the stiffness given by Eq. (21) with that obtained from the modal parameters (Eq. (59)). The stiffness $EI^{*}(\omega, T)$ at 20 ºC, 30ºC and 40ºC calculated with Eq. (21) and that obtained with Eq. (59) are presented in Figure 6, where it can be observed that the stiffness calculated with Eq. (21) underestimates the stiffness at all temperatures in all the frequency range. Moreover, the discrepancies increase with increasing temperature.

The stiffness calculated with modal parameters can only be estimated at the natural frequencies and the curves shown in Figure 6 have been fitted with splines.

The stresses at 40ºC were recalculated using the experimental stiffness determined with Eq. (59) (see Figure 6). The new results are shown in Figure 7, the errors being less than 6%. This demonstrates that the technique provide accurate results if good measurements are carried out and accurate mechanical properties of the glass and PVB are used in the analytical calculations.

6 CONCLUSIONS

In the practical calculations of laminated glass elements, as well as in preliminary designs, it is very useful to consider simplified methods. In the last years, several equations have been proposed to calculate displacements, internal forces, stresses, etc., in laminated glass beams and plates under static loads using the effective thickness concept [2, 8, 25]. Recently, Aenlle and Pelayo [15, 16] have derived a dynamic effective thickness for predicting the modal parameters (natural frequencies, mode shapes and damping ratios) in laminated glass beams and plates.

In this paper a dynamic effective thickness to estimate stresses in laminated glass beams under dynamic loadings in the frequency domain has been derived using the correspondence principle [20, 21, 22, 23]. With this technique, the stresses can be estimated using a monolithic model, avoiding the use of layered finite element models or complicated analytical models. The equations have been derived for three layered laminated glass beams with glass showing a linear elastic behaviour and the polymeric core showing viscoelastic behaviour. The stresses in time domain can be easily computed by inverse Fourier Transform [36].

The concepts of dynamic effective Young Modulus and dynamic effective distance to the neutral axis have also been proposed as an alternative to the effective thickness which can be used when the curvature of the beam is known from analytical or numerical models or from experimental tests. However, the effective thickness has to be used with Eqs. (41) and (42), i.e. when we want to use the bending moment distribution. On the other hand, the effective Young modulus is more appealing for using in numerical and analytical models because the monolithic model has constant thickness whereas a time (or frequency) and temperature dependent Young modulus is defined.

The results provided by the proposed methodology can be improved using experimental data. If modal analysis is applied to the laminated glass beam in order to estimate the modal parameters, a better estimation of the effective stiffness $EI^*(\omega,T)$ can be obtained using Eq. (59) which, in turn, can be used in Eqs. (35-40) to obtain better effective distances to the neutral axis and effective Young modulus.

In order to validate the methodology, the stresses of a laminated glass beam with the following geometrical data: $\mathrm{L} = 1$ m, $\mathrm{H}_1 = 3.75$ mm, $\mathrm{H}_2 = 0.38$ mm, $\mathrm{H}_3 = 7.90$ mm, $\mathrm{b} = 0.1$ m, with annealed glass and PVB core, were estimated using the dynamic stress effective thickness. The analytical predictions were validated by experimental tests carried out in the temperature range from 20 to 40 $^{\mathrm{o}}\mathrm{C}$ with simply supported and free-free boundary conditions. For temperatures below 20 $^{\mathrm{o}}\mathrm{C}$ the mechanical behaviour of the laminated glass is similar to a monolithic material and the technique is very accurate. The beam was excited with an impact hammer applying hits random in time and space. The stresses were estimated using Eqs. (57) and (58) and the analytical predictions were compared with the experimental ones measured with strain gages. It has been demonstrated that the proposed technique allows estimating stresses in laminated glass beams with a good accuracy. The discrepancies between the analytical and the experimental stresses for both the simply supported and the free configurations decrease significantly (error less than a 6%) when accurate mechanical properties of PVB and glass are used.

ACKNOWLEDGMENTS

The economic support given by the Spanish Ministry of Education through the project BIA2011-28380-C02-01 and BIA2014-53774-R are gratefully appreciated.

REFERENCES

[1] Ferry, J.D., Viscoelastic Properties of Polymers, Third ed., John Wiley & Sons, Ltd., New York. 1980.

[2] Benninson, S., M.HX, Q. and Davies, P., High-performance laminated glass for structurally efficient glazing. Innovative Light-weight Structures and Sustainable Facades, Hong Kong, May, 2008.

[3] Asik, M.Z., Tezcan, S., A Mathematical Model for the Behaviour of Laminated Glass Beams, Comput Struct. 2005;83:1742-1753.

[4] Norville, H.S., King, K.W., and Swoord, J.L., Behaviour and strength of laminated glass, J Eng Mech. 1998;124(1):46-53.

[5] Ivanov, I.V., Analysis, Modeling and Optimization of Laminated Glasses as Plane Beam, Int J Solids Struct, 2006;43(22-23):6887-6907.

[6] Koutsawa, Y., and Daya, E.M., Static and Free Vibration Analysis of Laminated Glass Beam on Viscoelastic Supports, Int J Solids Struct, 2007;44:8735-8750.

[7] Calderone, I., Davies, P.S., and Benninson, S.J., Effective Laminate Thickness for the Design of Laminated Glass. *In: Glass Processing Days*, Tampere, Finland, 2009.

[8] Galuppi, L., and Royer-Carfagni, G.F., Effective Thickness of Laminated Glass Beams: New Expression via a Variational Approach, J Struct Eng, 2012;38:53-67.

[9] Ross, D., Ungar, E.E., and Kerwin, E.M., Damping of Plate Flexural Vibrations by Means of Viscoelastic Laminate, Structural Damping, ASME, 1959; p. 49-88.

[10] DiTaranto, R.A., and McGraw, Jr, J.R., Vibratory Bending of Damped Laminated Plates, J Eng Ind, 1969;91(4):1081-1090.

[11] DiTaranto, R.A., Theory of Vibratory Bending for Elastic and Viscoelastic Layered Finite-Length Beams, J Appl Mech, 1965;32:881-886.

[12] Mead, D.J., and Markus, S., The Forced Vibration of a Three-Layer, Damped Sandwich Beam with Arbitrary Boundary Conditions, J Sound Vib, 1969;10(2):163-175.

[13] Mead D.J., and Markus, S., Loss Factors and Resonant Frequencies of Encastré Damped Sandwich Beam, J Sound Vib, 1970;12(1):99-112.

[14] Rao, D.K., Frequency and Loss Factors of Sandwich Beams under Various Boundary Conditions, J Mech Eng Sci, 1978;20(5):271-282.

[15] López-Aenlle, M., Pelayo, F., Frequency Response of Laminated Glass Elements: Analytical Modelling and Effective Thickness, Appl Mech Rev, 2013;65(2), 020802 (13 pages).

[16] M. López-Aenlle and Pelayo, F. Dynamic effective thickness in laminated-glass beams and plates, Compos Part B-Eng, 2014;67:332-347.

[17] López-Aenlle, M., Pelayo, F., Villa, L.M., Barredo, J., Hermanns, L. and Fraile, A., Operational Modal Analysis on Laminated Glass Beams. In proc. Of the 4th International Operational Modal Analysis Conference (IOMAC11). Istambul, 2011.

[18] Pelayo, F., López-Aenlle, M., Hermanns, L. and Fraile, A., Modal Scaling of a Laminated Glass Plate. In Proc. Of the 5th International Operational Modal Analysis Conference (IOMAC), Guimaraes, 2013, paper 175.

[19] Blasón, S., López-Aenlle, M., Pelayo, F., Influence of Temperature on the Modal Parameters of Laminated Glass Beams, In Proc. Of the International Conference on Vibration Problems (ICOVP13). Lisbon, 2013, paper-504, p. 270.

[20] Lee, E.H., Stress Analysis in Viscoelastic Bodies, Q J Mech Appl Math, 1955;13:183-190.

[21] Read, W.T., Stress Analysis for Compressible Viscoelastic Materials. J Appl Phys, 1950;21:671-674.

[22] Tschoegl, N.W., The Phenomenological Theory of Linear Viscoelastic Behaviour, Springer-Verlag, Berlin. 1989.

[23] Lakes, R. S. (2009). Viscoelastic materials. Cambridge: Cambridge University Press.

[24] Williams, M.L., Landel, R.F., and Ferry, J., The Temperature Dependence of Relaxation Mechanisms in Amorphous Polymers and Other Glass-forming Liquids, J Am Chem Soc, 1955;77:3701-3707.

[25] Galuppi, L., Manara, G. and Royer-Carfagni, G., Practical expressions for the design of laminated glass. Compos Part B-Eng, 2013;45:1677-1688.

[26] Galuppi, L., and Royer-Carfagni, G.F., Laminated Beams with Viscoelastic Interlayer, Int J Solids Struct, 2012;49(18):2637-2645.

[27] Kerwin, E.M., Damping of Flexural Waves by a Constrained Viscoelastic Layer, J. Acoust. Soc. Am, 1959;31(7):952-962.

[28] Pelayo, F., Aenlle, M. L., Brincker, R. and A. Fernández-Canteli. Stress estimation in structures using operational model analysis. Third International Operational Modal Analysis Conference (IOMAC), 2009; 675-682.

[29] Rune Brincker, Anders Skafte, Manuel López-Aenlle, Aldo Sestieri, Walter D'Ambrogio, Alfonso Canteli, A local correspondence principle for mode shapes in structural dynamics, Mech Syst Signal Pr, 2014;1(3):91-104.

[30] Maia N, Silva J, He J, Lieven N, Lin R-M, Skingle, G, To W, Urgueira A (1997) Theoretical and Experimental Modal Analysis. Research Studies Press Ltd.

[31] Brincker, R.; Ventura, C. & Andersen, P. Why output-only modal testing is a desirable tool for a wide range of practical applications In Proceedings of the International Modal Analysis Conference (IMACXXI), 2003.

[32] Brincker, R., Zhang, L-M., and Andersen. P., Modal Identification from Ambient Response Using Frequency Domain Decomposition, in: Proceedings of the 18th International Modal Analysis Conference (IMAC), San Antonio, 2000, p. 625-630.

[33] Van Overschee, P., and De Moor, B., Subspace Identification for Linear Systems: Theory, Implementation & Applications, Dordrecht, Netherlands, Kluwer Academic Publishers. 1996.

[34] Nashif, A.D., Jones, D.I.G., and Henderson, J.P., Vibration Damping. John Willey and Sons, New York. 1985.

[35] López-Aenlle, M. and Pelayo, F., The effective-thickness concept in laminated-glass elements under static loading. Eng Struct, 2013;56:1092-1102.

[36] E. Oran Brigham. The Fast Fourier Transform. Prentice Hall, 1974.

Figure captions:

Figure 1. Laminated glass beam section and schematic representation of the different layers.

Figure 2. Test setups used in the experiments.

Figure 3. Estimated and experimental stresses in point 1 at 20 ºC, 30 ºC and 40 ºC in simply-supported condition. Left: time history, Center: detail of the time history, Right: power spectral density.

Figure 4. Estimated and experimental stresses in point 2 at 20 ºC, 30 ºC and 40 ºC in simply-supported condition. Left: time history, Center: detail of the time history, Right: power spectral density.

Figure 5. Estimated and experimental stresses in point 1 at 20 ºC, 30 ºC and 40 ºC in free-free boundary condition. Left: time history, Center: detail of the time history, Right: power spectral density.

Figure 6. Estimated and experimental stiffness ($EI^*(\omega_{xp}, T)$) at 20 ºC, 30 ºC and 40 ºC.

Figure 7. Estimated and experimental stresses at $T = 40\ ^oC$ under free-free condition using the experimental stiffness ($EI^*(\omega_{xp}, T)$).

Table1

Table 1. Natural frequencies and loss factors for the glass beam under simply supported boundary conditions.

Temp.	Mode 1		Mode 2		Mode 3	
	Frequency	Loss factor	Frequency	Loss factor	Frequency	Loss factor
[^{o}C]	[Hz]	[%]	[Hz]	[%]	[Hz]	[%]
20	31.33	1.16	118.42	1.17	262.59	1.15
30	30.92	2.22	116.05	2.46	255.44	4
35	30.15	4.89	113.51	3.41	246.82	8.45
40	29.59	8.39	108.47	9.67	232.12	9.15

Table2

Table 2. Natural frequencies and loss factors for the glass beam under free-free boundary conditions.

Temp.	Mode 1		Mode 2		Mode 3	
	Frequency	Loss factor	Frequency	Loss factor	Frequency	Loss factor
[^{o}C]	[Hz]	[%]	[Hz]	[%]	[Hz]	[%]
20	66.47	0.56	182.0	0.97	354.5	1.20
30	65.97	2.11	179.3	3.75	346.4	5.30
35	65.37	4.56	175.9	9.40	335.5	11.85
40	63.70	8.98	168.1	22.98	311.8	19.54

Table3

Table 3. Contribution of the numerical modes in the expansion of the experimental mode shapes using the local correspondence principle.

Free-Free					
Experimental Mode	Numerical Modes				
	1	2	3	4	5
1	0.9844	0	0	0	0.0122
2	0	0.9896	0	0	0
3	0	0	0.9993	0	0
Simply - supported					
1	0.9913	0	0.0081	0	0
2	0.0072	0.9971	0	0.0076	0
3	0	0	0.9969	0.0154	0

Table 4. Errors between the predicted and the experimental stresses for the first mode at different temperatures in points 1 and 2.

Boundary Condition	Frequency [Hz]	Temperature [^{o}C]	Error [%] Point 1	Point2
Simply Supported	31.33	20	7.56	8.62
	31.05	25	7.97	5.37
	30.92	30	8.35	2.23
	30.15	35	16.45	6.58
	29.59	40	18.34	7.01
Free-Free	66.47	20	10.97	2.89
	66.12	25	12.14	11.95
	65.96	30	11.44	13.96
	65.37	35	17.84	19.22
	63.78	40	16.36	19.95

Figure1

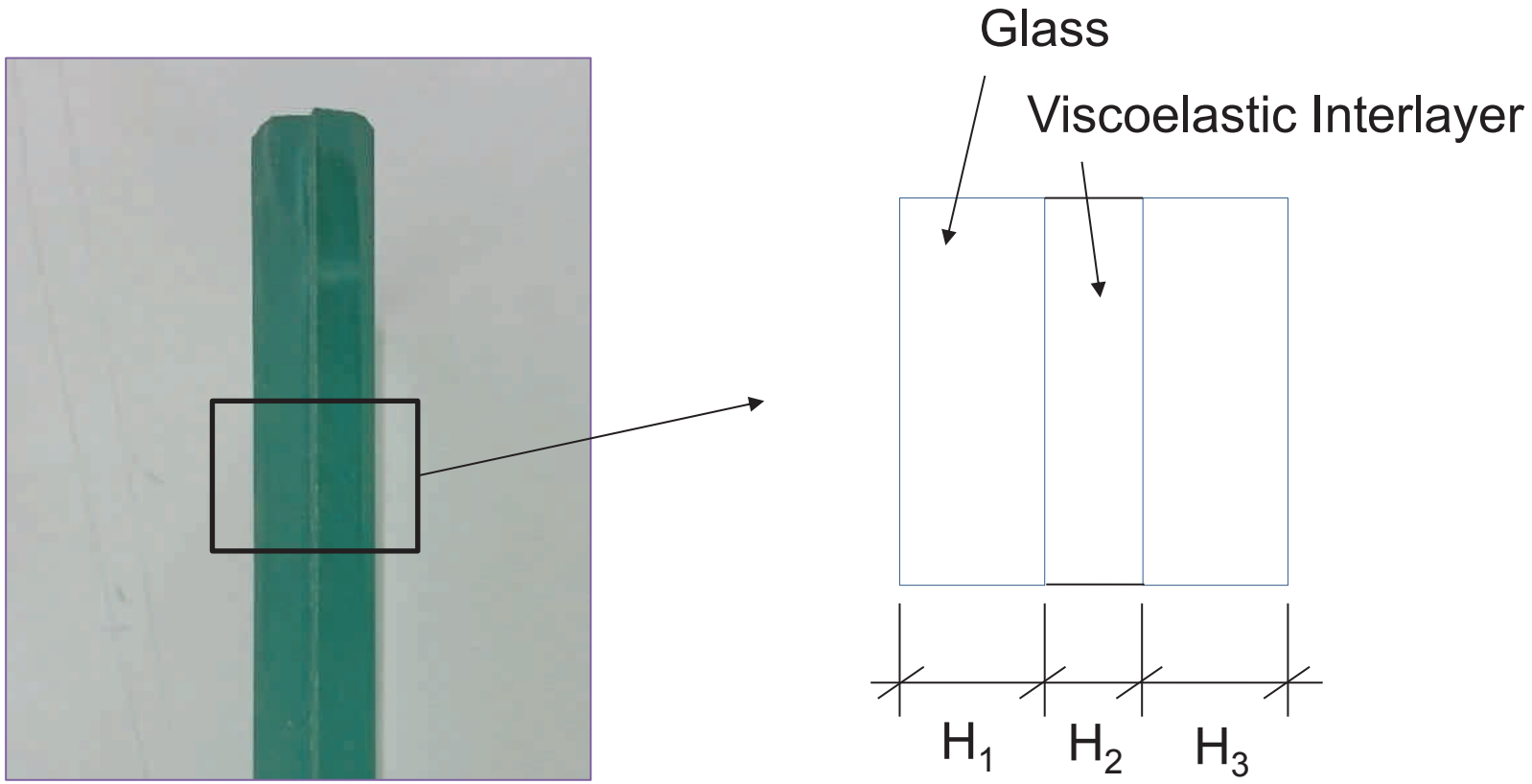

Figure2

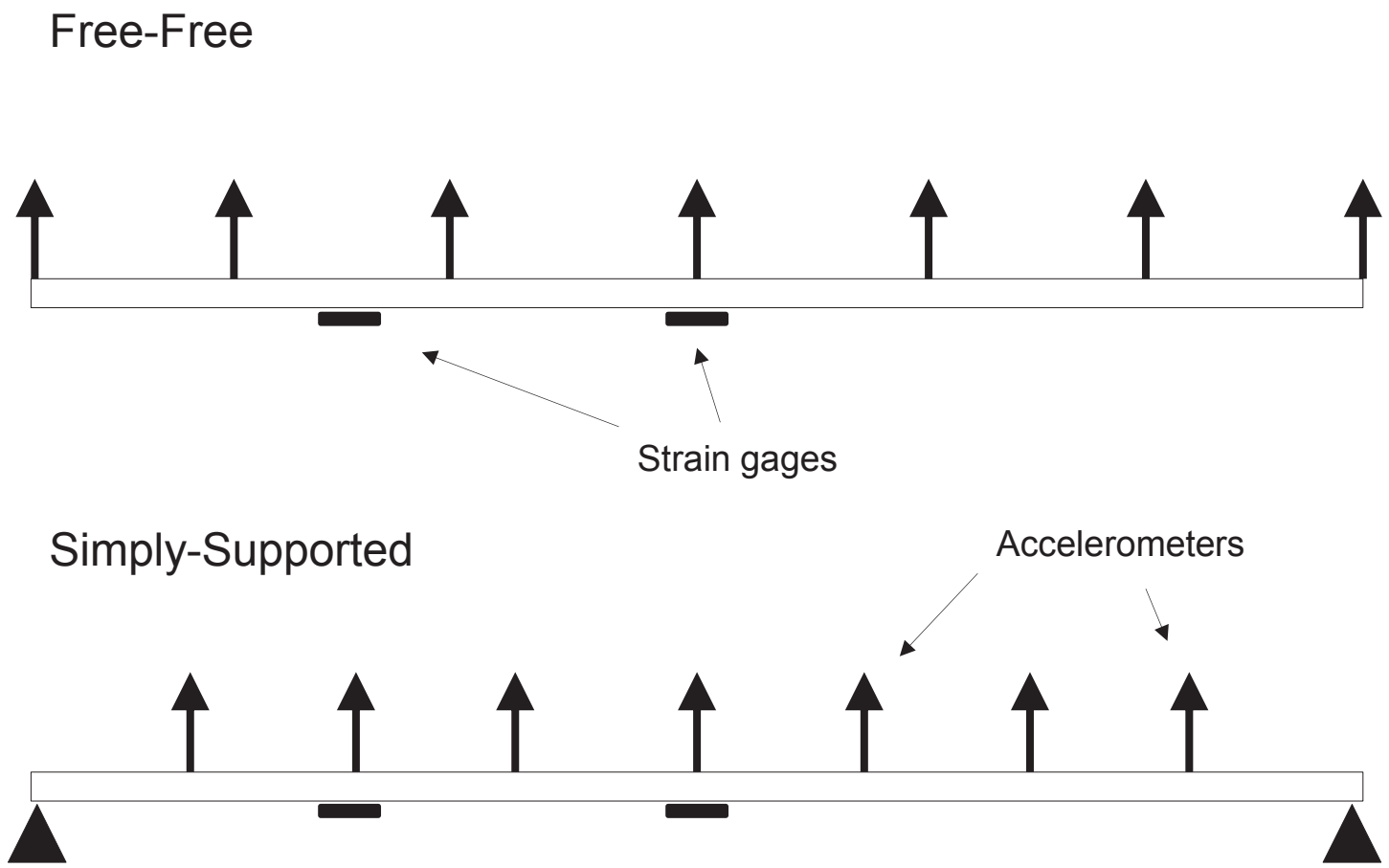

Figure3

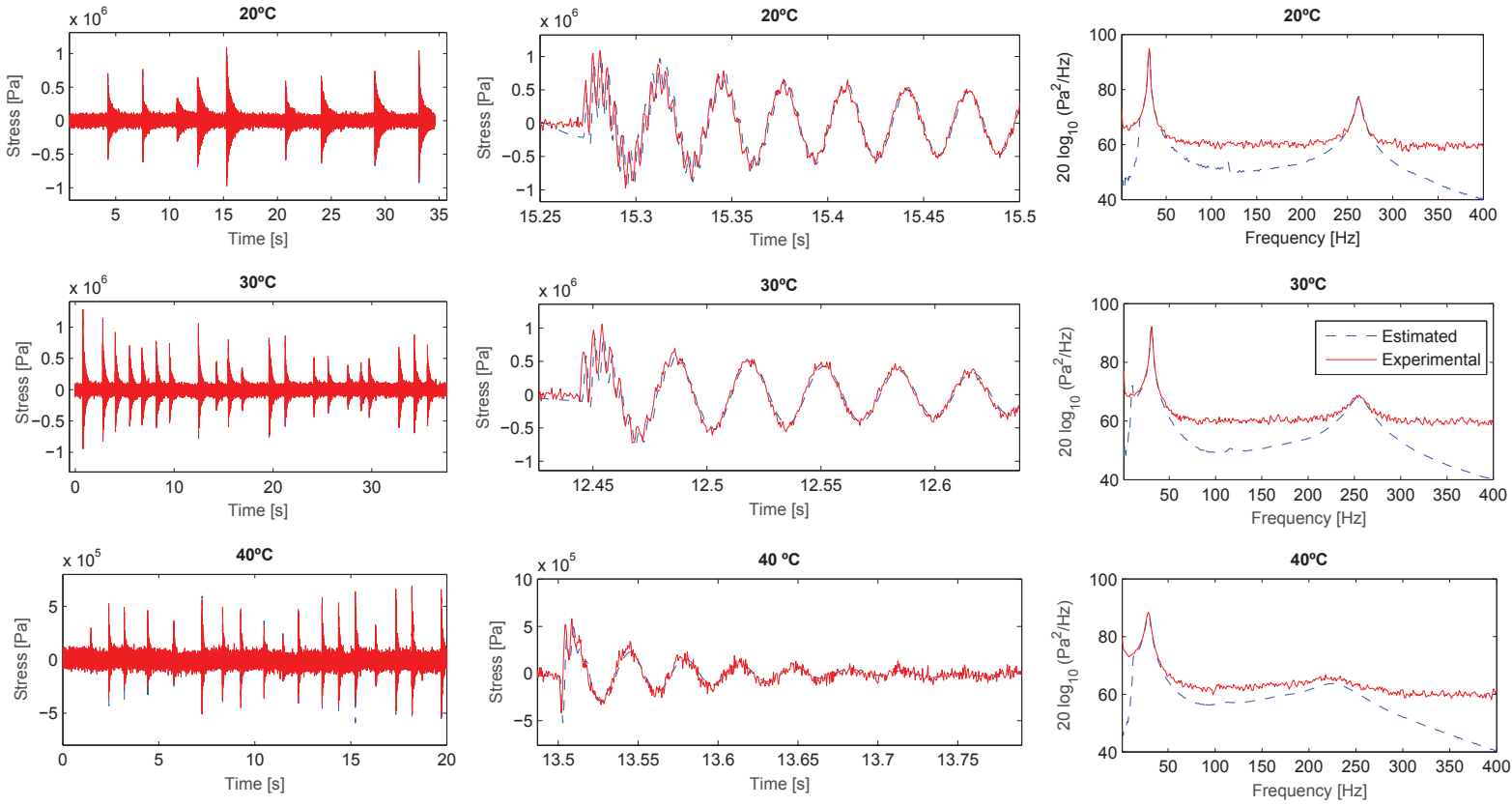
20ºC
x 10^6
Stress [Pa]
Time [s]
20ºC
x 10^6
Stress [Pa]
Time [s]
20ºC
20 log10 (Pa^2/Hz)
Frequency [Hz]
30ºC
x 10^6
Stress [Pa]
Time [s]
30ºC
x 10^6
Stress [Pa]
Time [s]
30ºC
Estimated
Experimental
20 log10 (Pa^2/Hz)
Frequency [Hz]
40ºC
x 10^5
Stress [Pa]
Time [s]
40 ºC
x 10^5
Stress [Pa]
Time [s]
40ºC
20 log10 (Pa^2/Hz)
Frequency [Hz]

Figure4

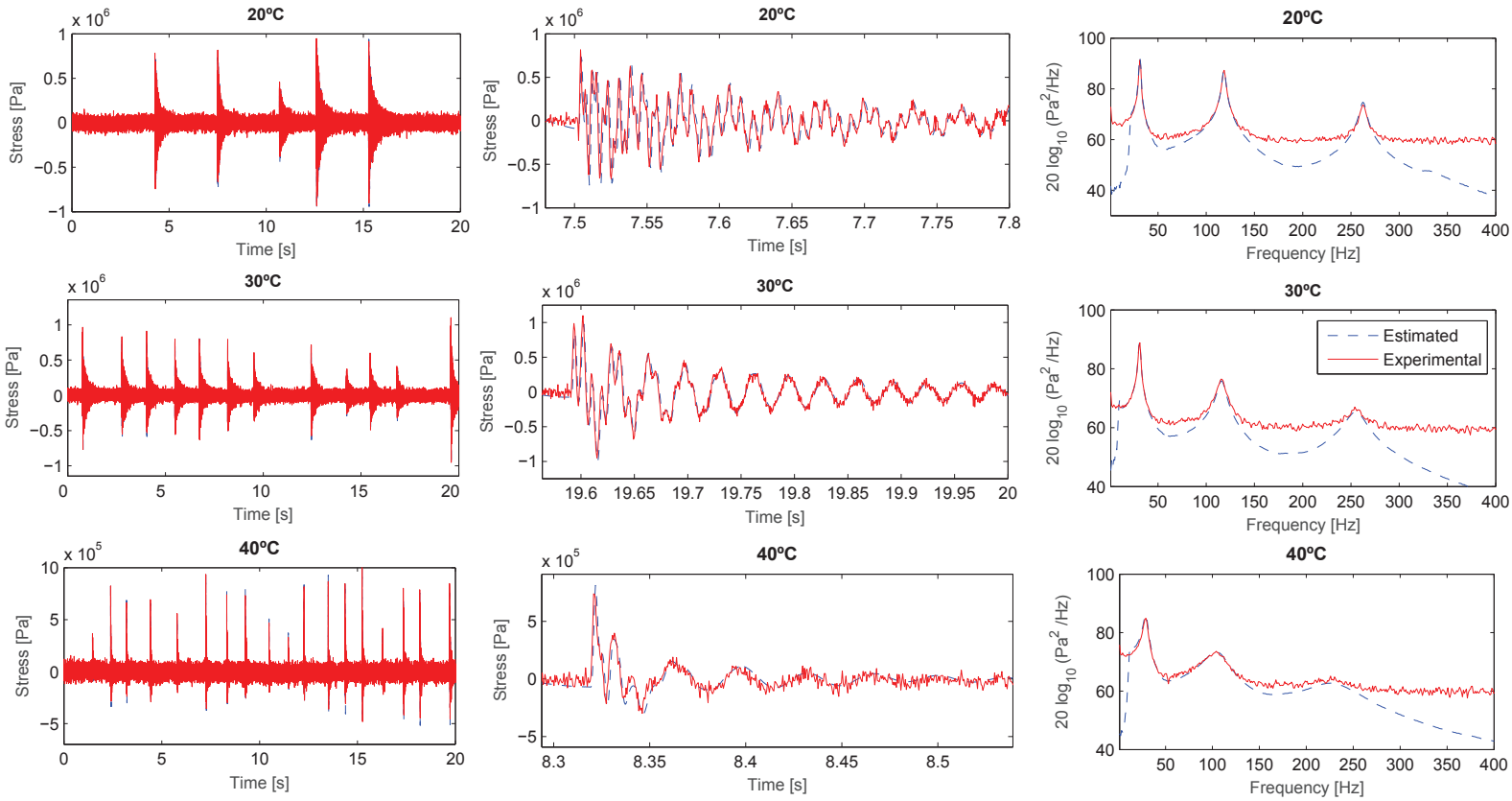
20ºC
x 10^6
Stress [Pa]
Time [s]
20ºC
x 10^6
Stress [Pa]
Time [s]
20ºC
20 log10 (Pa2/Hz)
Frequency [Hz]
30ºC
x 10^6
Stress [Pa]
Time [s]
30ºC
x 10^6
Stress [Pa]
Time [s]
30ºC
Estimated
Experimental
20 log10 (Pa2 /Hz)
Frequency [Hz]
40ºC
x 10^5
Stress [Pa]
Time [s]
40ºC
x 10^5
Stress [Pa]
Time [s]
40ºC
20 log10 (Pa2 /Hz)
Frequency [Hz]

Figure5

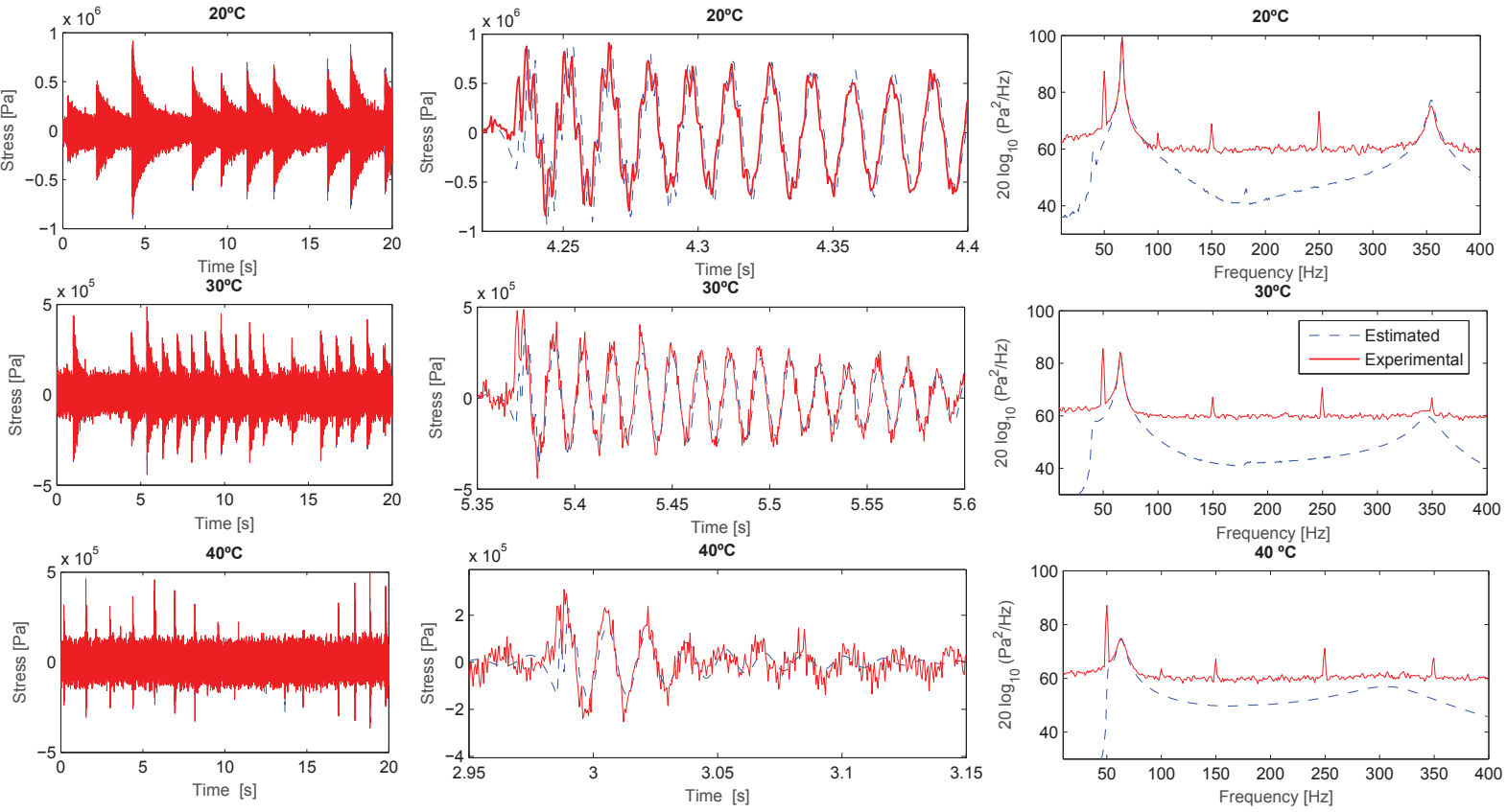
20ºC
x 10^6
Stress [Pa]
Time [s]
20ºC
x 10^6
Stress [Pa]
Time [s]
20ºC
20 log10 (Pa^2/Hz)
Frequency [Hz]
30ºC
x 10^5
Stress [Pa]
Time [s]
30ºC
x 10^5
Stress [Pa]
Time [s]
30ºC
Estimated
Experimental
20 log10 (Pa^2/Hz)
Frequency [Hz]
40ºC
x 10^5
Stress [Pa]
Time [s]
40ºC
x 10^5
Stress [Pa]
Time [s]
40 ºC
20 log10 (Pa^2/Hz)
Frequency [Hz]

Figure6

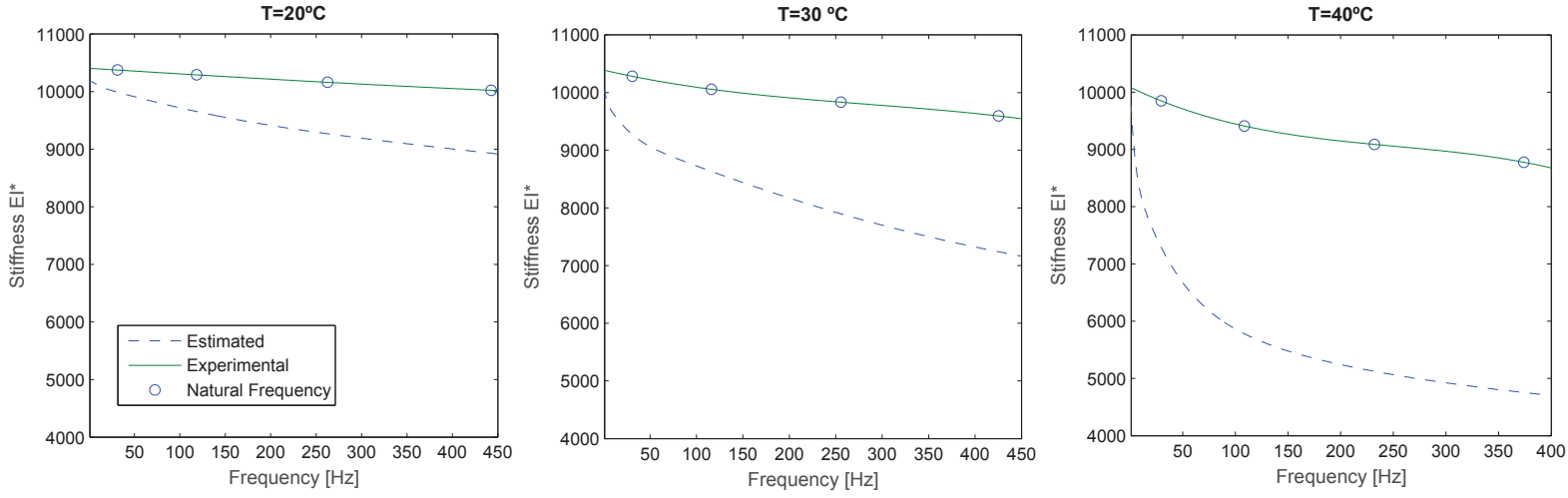
T=20ºC
T=30 ºC
T=40ºC
Stiffness EI*
Frequency [Hz]
Estimated
Experimental
Natural Frequency
11000
10000
9000
8000
7000
6000
5000
4000
50
100
150
200
250
300
350
400
450

Figure7

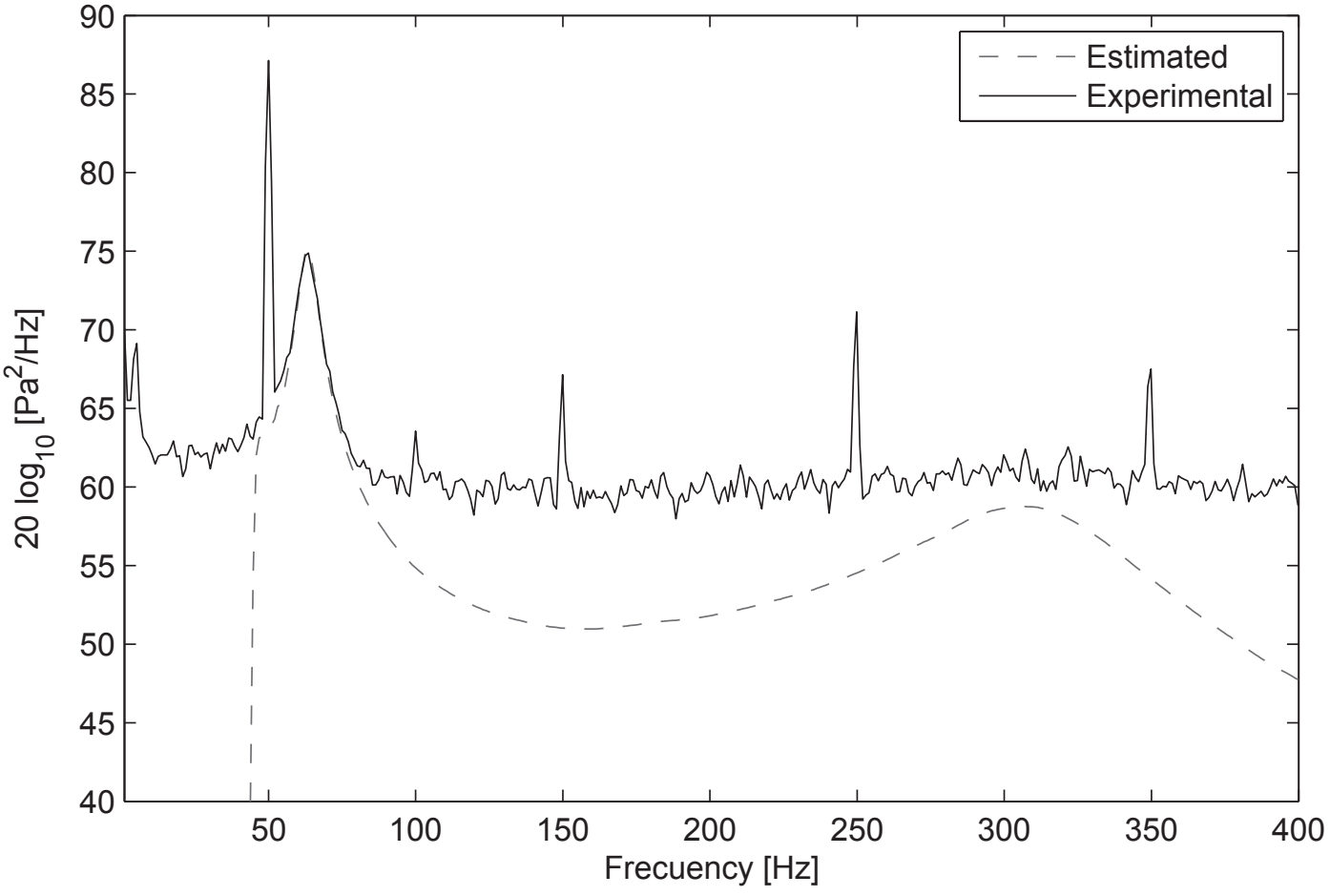
Estimated
Experimental
90
85
80
75
70
65
60
55
50
45
40
20 log10 [Pa2/Hz]
50
100
150
200
250
300
350
400
Frecuency [Hz]